Energy Reports 11 (2024) 1399–1411

Contents lists available at ScienceDirect

Energy Reports

journal homepage: www.elsevier.com/locate/egyr

Research paper

Impact of turbine availability and wake effect on the application of dynamic thermal rating of wind farm export transformers

Zhongtian Li [a,*], Patrik Hilber [a], Tor Laneryd [b], Gonzalo Pablo Navarro Diaz [c], Stefan Ivanell [c]

[a] Department of Electromagnetic Engineering, School of Electrical Engineering and Computer Science, KTH Royal Institute of Technology, Stockholm, Sweden
[b] Hitachi Energy Research, Västerås, Sweden
[c] Department of Earth Sciences, Wind Energy Section, Uppsala University, Visby, Sweden

ARTICLE INFO

Keywords:
Wake effect
Turbine availability
Transformer loading
Transformer aging
Wind farm reliability

ABSTRACT

Dynamic thermal rating allows transformers to operate beyond the nameplate rating according to the actual weather and loading conditions. This paper proposes a methodology to improve the application of this technology in the design of new transformers or in the operation of existing transformers connected to wind farms by accurately predicting their load profiles, accounting for the influence of wake effect and turbine availability. Specifically, the variation of turbine availability due to the intermittent wind is considered in the load profile estimation. Additionally, a correction method, which can be incorporated into any wake model, is proposed to improve the accuracy of wake loss computation. A case study shows that the wake effect and the changing turbine availability shorten the time that the transformers maintain at full load, thereby reducing the aging rate of the wind farm export transformers. The findings suggest that considering these two factors in the DTR application can benefit the longevity and efficiency of wind farm exported transformers.

1. Introduction

The European Union (EU) is accelerating its green energy transition with the objective of reducing the dependence on fossil fuels. The "Marienburg Declaration" (Anon, 2022b) and the "Esbjerg Offshore Wind Declaration" (Anon, 2022a) signed in 2022 set ambitious goals to increase the installed capacity of offshore wind farms significantly in the following decade. The high penetration of wind power and increasing electricity demands require an upgrade or expansion of the existing transmission networks, which is hindered by the high investment costs and long construction cycles (Teh et al., 2018). If the power transmission is to be improved with the existing grid, the regulated loading limit of grid infrastructure, which is called static thermal rating (STR), becomes the constraint.

Static thermal rating (STR) is a traditional method to rate power transmission components such as overhead lines, transformers and cables. Regarding to transformers, their expected lifespan can be considered a function of insulation degradation (Hillary et al., 2017) and related to working temperature. For instance, for a transformer at the planning stage, STR assumes a constant load and sets a constant thermal limit to ensure its safe operation under the "worst-case" environment conditions (Susa et al., 2005) without continuous monitoring. However, in the wind farm scenario, STR restricts the efficient utilization of wind farm export transformers (WFETs) due to the intermittent nature of wind, ambient temperature and air cooling effect. Power transformers limited by STR are typically loaded at 40%−60% of their actual capacity to guarantee their reliability during contingencies (Humayun et al., 2015), which results in a lower aging rate and much longer remaining lifetime compared to the initial design estimation (Anon, 2012). In Sweden, the operation lifetime of wind turbines typically ranges from 20 to 25 years (Pakenham et al., 2021; Anon, 2016), whereas the economic lifespan of the transformers is in the range of 50 years (Anon, 2018a).

The underutilized transformers cause unnecessary expenditure and complicate the evaluation of their remaining life expectancy. Compared to an expansion of new transmission grids, dynamic thermal rating (DTR) provides an alternative to make better utilization of the existing transmission systems. DTR enables transformers (especially mineral-oil-immersed type (Arguence and Cadoux, 2020; Tripathy and Lakervi, 2005; Simonson and Lapworth, 1995)) to operate beyond their nameplate rating while still adhering to their thermal limits (Lachman et al., 2003).

In the existing literature, most works focus on discussing the benefits of applying DTR in transmission components (Turnell et al., 2018; Zarei et al., 2019) and how to further optimize the power system operation with DTR (Viafora et al., 2019; Akhlaghi et al., 2022; Li et al., 2023). However, few previous papers discuss in detail about how

* Corresponding author.
E-mail address: zhonli@kth.se (Z. Li).

https://doi.org/10.1016/j.egyr.2023.12.042
Received 10 December 2022; Received in revised form 14 December 2023; Accepted 19 December 2023
Available online 13 January 2024

Nomenclature

BD	Binomial distribution
DTR	Dynamic thermal rating
HST	Hot spot temperature
MSE	Mean square error
MTBF	Mean time between failure
MTTR	Mean time to repair
NO	non-operative state
OOS	out of service state
PA	Production-based availability
STR	Static thermal rating
TOT	Top oil temperature
WFET	Wind farm export transformer (oil-immersed)
WIF	Wake impact factor
WMSE	Weighted mean square error
WT	Wind turbine
λ	Failure rate of wind turbine
μ	Repair rate of wind turbine
N	Total number of wind turbines
n	Number of failures in the measured intervals
p	Unavailability of wind turbine, $p = 1 - q$
q	Availability of wind turbine
T	Number of measured intervals in the data
$U_{\text{cut-in}}$	Lower limit of wind speed at which the turbine starts generating electricity, unit: m/s
$U_{\text{cut-out}}$	Upper limit of wind speed at which the turbine stops generating electricity, unit: m/s
U_{ind}	Reduced wind speed of each individual turbine due to the wake effect, unit: m/s
U_{rated}	Wind speed at which the turbine starts producing its maximum power, unit: m/s
Z	Number of intervals for which the turbines are out of service

to apply DTR in wind farm export transformers (WFETs). Due to the structure complexity of transformers compared with overhead lines and cables, it is not analyzed thoroughly yet how to apply DTR to transformers. It is indicated in Turnell et al. (2018), Li et al. (2021b), Viafora et al. (2019), Kazmi et al. (2021), Lai and Teh (2022) that the aging rate of transformers are highly influenced by the load profile and the ambient temperature. Without considering the factors influencing the load profile, applying DTR may put the transformer insulation at risk of accelerating aging and mechanical deterioration, which reduce the lifespan of transformers below expectation (Anon, 2012). Nonetheless, few research works discuss how to implement reliable estimation of the load profiles of transformers to ensure safe operation.

There are multiple factors influencing the estimation of the load profiles of WFETs, which can be classified as weather conditions (e.g. icing, wind speed and ambient temperature (Iskender and Mamizadeh, 2011; Daminov et al., 2021)) and loading conditions (e.g. turbine availability (Kazmi et al., 2021), wake loss (Li et al., 2021a)). In terms of loading conditions, the impact of the wake effect and the turbine availability on the load profile of the transformers connected to the wind farms is not analyzed thoroughly.

Regarding the wake effect, only the results in Li et al. (2021a) show that the estimated load profile considering the wake effect is closer to the measured loading data than if it is not considered. Wake effect is the phenomena where downstream turbines suffer the increased turbulence and extraction of energy form the upstream turbines (Manwell et al., 2010). The wake effect occurs as long as more than one turbine is in operation on the wind farm. When estimating the wake loss to avoid an overestimation of wind power output (de Sá Sarmiento et al., 2022; Porté-Agel et al., 2020), the influence of wind speed and direction (Wang et al., 2022; Zhan et al., 2020) and wind farm layout (Yang et al., 2019) are considered in this paper. While atmospheric stability (Guo et al., 2021; Radünz et al., 2021) is not discussed here, the analysis of data on wind speed and direction still reveals the impact of the atmospheric stability on the wake loss. The first wake model was proposed by Jensen in Jensen (1983) and refined in Katic et al. (1986). It is a simplified one-dimensional analytical wake model (Jensen, 1983) assuming the wake effect is linearly expanding. Due to its simplicity, the Jensen model and its refined model are widely used in the planning of wind farm layout (Kim et al., 2012; Long and Zhang, 2015; Hou et al., 2015; Song et al., 2016) and the connected transmission system (Wu et al., 2013; Yang et al., 2015; Hou et al., 2016; Tao et al., 2020). However, the impact of the wake effect on the design and operation of the transmission components connected to wind farms, especially transformers, is not discussed in detail in the papers above.

Regarding turbine availability, few papers link it with the load profiles of WFETs except in Kazmi et al. (2021), in which the turbine availability is assumed as a constant when building a probabilistic model to estimate the annual load profile of a WFET. Nevertheless, the previous studies still provide valuable information on how turbine availability influences wind power generation (Sulaeman et al., 2017; Nguyen et al., 2019) and how to build probabilistic models to estimate the load profile of WFETs considering the turbine availability (Sayas and Allan, 1996; Karki et al., 2006; Leite et al., 2006; Manco and Testa, 2007; Nguyen and Mitra, 2017; Bhaumik et al., 2018). However, as Sulaeman et al. (2017), Nguyen et al. (2019) indicates, the turbine availability varies due to the intermittent nature of wind. Under high wind speed, it is unclear if the transformers suffer accelerating aging due to full loading or if the aging of transformers is reduced due to the variation of the turbine availability. Hence, the variation of the turbine availability due to the intermittent wind cannot be ignored when evaluating the load profile of WFETs.

It can be observed that the impact of the factors (wake effect and turbine availability) on the load profile of WFETs, is crucial to be analyzed when applying DTR to WFETs but has not been well implemented in the previous papers. In this paper, a methodology is introduced to consider the wake effect and the turbine availability in the load profile estimation of WFETs. The accuracy of the proposed methodology is verified by the measured data from an onshore wind farm located in the north of Sweden. Furthermore, the impact of the turbine availability and the wake effect on the load profile of the WFETs is assessed.

Compared to the existing research works, the main contribution of this paper can be summarized as follows. A methodology is proposed to assess the impact of wake effect and turbine availability on the load profile and aging rate of WFETs. Regarding the wake effect part, a Wake Impact Factor (WIF) correction method is proposed to correct the measured data to improve the accuracy of wake loss estimation. The proposed WIF method can be incorporated into any wake model and it requires wind data from only one turbine to estimate the wind speed of the rest turbines on the wind farm. Regarding the turbine availability part, a Markov model is proposed to consider the influence of the turbine availability in the load profile estimation of WFETs. The impact of wind speed on the change of turbine availability is taken into account.

The rest of this paper is organized as follows. Methodology description and modeling are given in Section 2. Section 2.1 illustrates how to implement the correction method in the wake loss computation.

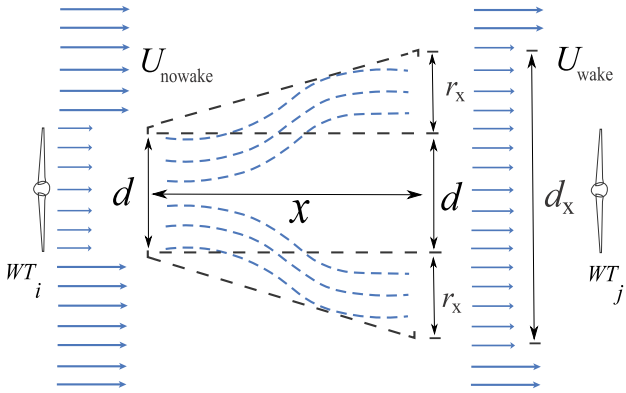

Fig. 1. Jensen wake model applied to two interacting turbines.

Section 2.2 explains the principle of the proposed Markov model and how to consider the variable turbine availability in the estimation. Section 2.3 exhibits the transformer thermal model. Section 3 presents the analysis of the data resource and a case study to verify the accuracy of the proposed model. Finally, this paper is ended with conclusions in Section 4.

2. Methodology

2.1. Estimation of wake effect

2.1.1. Jensen model

Compared to the Jensen model, the wake models in Larsen (1988), Ishihara et al. (2004), Frandsen et al. (2006), Yang and Sotiropoulos (2016) generate more accurate results at the price of high computational costs, which is not suitable for the scenario and time horizon in this paper. Hence, the Jensen wake model is used in this paper to consider the power loss caused due to the wake effect considering its simplicity. The model principle is shown in Eq. (1) and Fig. 1. Assuming θ_{nowake} (the direction of the incoming wind) is not changed, the reduced wind speed U_{wake_j} (m/s) of the jth turbine considering the wake effect due to other turbines is calculated based on the speed of the incoming wind U_{nowake} (m/s).

$$U_{\text{wake}_j} = U_{\text{nowake}}[1 - \sum_{i=1}^{N-1}(1 - \sqrt{1 - C_t})(\frac{d}{d_{X_i}})^2] \tag{1}$$

In Eq. (1), U_{nowake} is the incoming wind speed of the whole wind farm and U_{wake_j} is the downstream wind speed of WT_j considering the cumulative wake effect of the rest $(N-1)$ turbines. C_t is the thrust coefficient of the wind turbine, d_{X_j} is the diameter of the expanded wake area, which equals to,

$$d_{X_j} = d + 2r_{x_j} = d + 2kx_j \tag{2}$$

where d is the rotor diameter and x_j is the distance between WT_j and WT_i. A wake decay constant $k = 0.075$ is used in this onshore wind farm scenario (Zigras and Moennich, 2006). The wind shade effect due to upstream obstacles (turbines) is ignored.

2.1.2. Wake impact factor correction

For a wind farm in operation, a rough method to estimate the wind power generation is to use the average value of the measured wind speed from all turbines. The average value is used to minimize the impact of the wake effect on the estimation accuracy. However, the estimation using the average value differs from the real case. It is also challenging to collect accurate measured data from all turbines (due to the offline of some anemometers). Commonly, only data from a limited number of turbines is of high quality. A wake impact factor (WIF) correction method is proposed to solve this issue. This correction method requires wind data from only one turbine from the wind farm and the wind farm layout to estimate the wind speed of other turbines considering the influence of the wake effect.

In order to estimate the diminished wind speed of each turbine on a wind farm, U_{nowake} used in the Jensen model must be the incoming wind speed for the entire wind farm, in other words, the upstream wind for all turbines. The measured wind from the anemometer of one turbine can be upwind or downwind for other turbines on the wind farm depends on the wind direction and the location of the anemometer. Hence, the wind data measured by the anemometers (on the meteorological tower or on the turbine nacelle) is not usable directly as input for the Jensen model since the wind may have already suffered reduction before the measurement due to the wake effect. It is unclear if the measured wind speed from one turbine is upstream or downstream with regard to the rest turbines on the wind farm due to the changes in wind direction.

The intention of the wake impact factor correction (WIF) method is to correct the measured data before the data is proceeded with the Jensen model. The WIF method only requires wind speed from one turbine and can correct the wind speed from the "non-incoming" direction. Before the data is input to the Jensen model, it needs to be corrected to the incoming wind speed for the whole wind farm using the WIF method.

Initially, it is assumed that U_{mea_j} represents the measured wind speed from the anemometer of the jth wind turbine (WT_j). A test incoming wind speed U_{nowake} (with a variable wind direction θ_{nowake}) is defined in a certain range. This step aims to evaluate the influence of the wind farm layout on U_{nowake} before U_{nowake} reaches WT_j. The combination of U_{nowake} and θ_{nowake} in the defined range include all possible cases of wind. Using the Jensen wake model, the reduced wind speed U_{wake_j} of WT_j under all possible wind conditions can be calculated. After U_{wake_j} is derived based on U_{nowake} and θ_{nowake}, the wake impact factor (WIF) for the wind farm under different wind conditions is calculated using Eq. (3).

$$\text{WIF}_{\{U_{\text{mea}_j}, \theta_{\text{nowake}}\}} = \frac{U_{\text{wake}_j}}{U_{\text{nowake}}} \tag{3}$$

Assuming the imported wind direction θ_{nowake} is not changed, the wind speed U_{mea_j} from WT_j can be corrected to the corresponding incoming wind speed $U_{\text{nowake(wif)}}$ for the whole wind farm using Eq. (4).

$$U_{\text{nowake(wif)}} = \frac{U_{\text{mea}_j}}{\text{WIF}_{\{U_{\text{mea}_j}, \theta_{\text{nowake}}\}}} \tag{4}$$

2.1.3. Wind power evaluation

After the corrected incoming wind speed $U_{\text{nowake(wif)}}$ is calculated using the WIF method, Eq. (1) is used again to calculate the reduced wind speed $U_{\text{wake(wif)}}$ of each turbine to estimate the generated power from the wind farm. The power curve of the chosen turbine is used to estimate the power output from the turbine based on the wind speed. The corrected wind speed $U_{\text{wake(wif)}}$ of each turbine is fitted into the power curve to get the corresponding real-time power output P_{indiv}. The ideal real-time power output $P_{\text{out(est)}}$ on the condition that all turbines are in operation is calculated as,

$$P_{\text{out(est)}} = P_{\text{indiv}} N \tag{5}$$

Since the final objective of the paper is to operate transformers according to the thermal limit, the load factor is chosen to represent the load profile of transformer, similar to the setting in Arguence and Cadoux (2020). The total power output P_{out} from the wind farm is converted into load factor K, which is a ratio between load current I_{load} and rated current I_{rated}. This variable is an input in the calculation of the transformer operating temperature. If the voltage drop across the leakage reactance is ignored and the output voltage U is assumed as

a constant, K can be expressed by the generated power using Eq. (6). The denominator P_{rated} is the rating of the selected-size transformer and the numerator P_{load} depends on the real-time generated power from the wind farm.

$$K = \frac{I_{\text{out}}}{I_{\text{rated}}} = \frac{P_{\text{out}}/U}{P_{\text{rated}}/U} = \frac{\sum_{i=1}^{N} P_{\text{indiv},i}}{P_{\text{rated}}} \tag{6}$$

Load factor can also be used to check the simulation accuracy by comparing the results between the simulation duration curve K_{SIM} and the measurement duration curve K_{real}. Mean-squared error (MSE) is used as an indicator to evaluate the quality of simulation result compared to the measured data.

$$\text{MSE} = \frac{1}{n}\sum_{i=1}^{n}(K_{\text{SIM}_i} - K_{\text{real}_i})^2 \tag{7}$$

Since this paper focuses on the influence of the wind power on the transformer insulation, more attention should be paid to when the transformer load is high. Hence, an weighted factor $w_i = K_{\text{real}_i}$ is added to neutralize the influence of zero values in the load factor. The weighted mean square error (WMSE) is calculated to evaluate the simulation accuracy.

$$\begin{aligned}\text{WMSE} &= \frac{1}{n}\sum_{i=1}^{n} w_i(K_{\text{SIM}_i} - K_{\text{real}_i})^2 \\ &= \frac{1}{n}\sum_{i=1}^{n} K_{\text{real}_i}(K_{\text{SIM}_i} - K_{\text{real}_i})^2\end{aligned} \tag{8}$$

2.2. Turbine availability

Production-based availability (PA) is used in this section for the estimation of the transformer load. It is a simplified index to evaluate the availability of turbines when the wind speed u_{ind} satisfies the requirement of power generation. When $U_{\text{cut-in}} \le u_{\text{ind}} \le U_{\text{cut-out}}$, the corresponding WT is considered production-based unavailable if it cannot produce power in either out-of-service (OOS) mode or in non-operative (NO) mode according to standard (Anon, 2019). This definition considers the WT as a whole and aims to avoid confusion with the reliability of the wind turbines sub-assemblies. In this way, the availability of wind turbines can be combined with wind power prediction to improve the estimation of the transformer load.

To calculate the turbine availability, the failure and repair rate of turbines should be evaluated first. It has to be noted that the 'failure' here means the turbine stops rotation when the wind speed is in the range ($U_{\text{cut-in}} \le u_{\text{ind}} \le U_{\text{cut-out}}$) and the 'repair' means the whole process after the failure and before the turbine re-starts operation.

2.2.1. Failure & repair rate

After Type III data (the data influenced by the failure and maintenance of wind turbines) is included, the turbine availability should be taken into account. The wind turbines stop operation and cannot produce power during the failure or maintenance period. In this paper, the failure rate and repair rate is defined in a per turbine per year format.

A filter is defined to select the data in which the wind speed satisfies the condition of power generation ($U_{\text{cut-in}} \le u_{\text{ind}_i} \le U_{\text{cut-out}}$). It is assumed the repair is initiated immediately when the failure occurs. A data-based method is defined to calculate the failure and repair rate in Fig. 2. Based on n and Z derived in Fig. 2, the availability of the wind farm can be determined. For the wind turbine, which is a repairable system, the repair/down time cannot be ignored compared to the operating/up time. According to Carroll et al. (2014), Wallnerström and Hilber (2014), Spinato et al. (2009), Tavner et al. (2007), for a repairable system with data in hours, the yearly based MTTF, MTTR and MTBF can be expressed as.

$$\text{MTTF} = \frac{T - Z}{n} \tag{9}$$

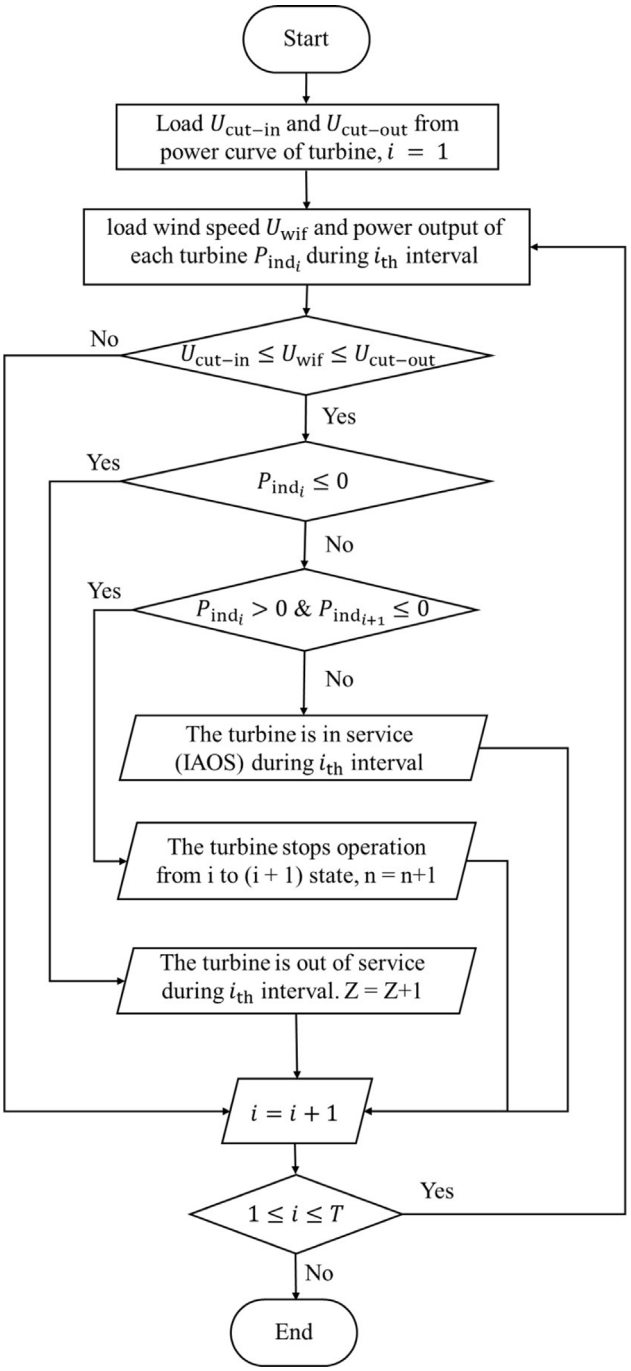

Fig. 2. Flow chart of defining n and Z to calculate failure and repair rate.

$$\text{MTTR} = \frac{Z}{n} \tag{10}$$

$$\text{MTBF} = \text{MTTF} + \text{MTTR} \tag{11}$$

The yearly based failure rate λ, repair rate μ and the availability q can be expressed as,

$$\lambda = \frac{1}{\text{MTBF}} \tag{12}$$

$$\mu = \frac{1}{\text{MTTR}} \tag{13}$$

$$q = \frac{\text{MTTF}}{\text{MTBF}} \tag{14}$$

2.2.2. Binomial distribution (BD) model

The binomial distribution (BD) equation is used to calculate the probability distribution of the number of running turbines based on a constant wind turbine availability q. The probability distribution that a certain number of turbines in operation is given by the binomial probability density,

$$A_x = \binom{N}{x} p^x q^{N-x} = \frac{N!}{(N-x)!x!} p^x q^{N-x} \tag{15}$$

where

- x is the number of real-time running turbines, varying from 0 to N
- p is the unavailability of wind turbine, $p = 1 - q$

Next, the uniform pseudo-random number generator in Matlab is used to generate a sequence of random number based on the binomial probability distribution, which simulates the variation of the real-time number of operational turbines N_{run} in time series. The improved estimated wind power output $P_{(\text{wif})+\text{BD}}$ from the wind farm, which considers the influence of turbine availability, can be calculated as:

$$P_{(\text{wif})+\text{BD}} = P_{\text{indiv}} N_{\text{run}} \tag{16}$$

2.2.3. Markov model

In the BD model, the variation of turbine failure and repair rate under different weather conditions is not considered. In reality, the failure rate and the repair rate of turbines are influenced by environmental conditions. The correlation between the wind speeds and the failure rates of turbine sub-assemblies is determined to be negative in Tavner et al. (2006). Based on this conclusion, a discrete Markov chain model is proposed in Nguyen et al. (2019) to take the variation of turbine availability under different weather conditions into consideration.

However, the turbine population considered in Tavner et al. (2006) is too large and spread unevenly over Denmark. Clearer correlations can be found between WT failures and weather data if a limited population of identical WTs at several locations is used (Tavner et al., 2013). Besides, the wake effect, an important factor influencing the turbine operation and power generation, is not considered in Nguyen et al. (2019). In this session, a new Markov-chain method considering the wake effect is proposed to check the correlation between the wind turbine availability and the wind speed of a wind farm with N wind turbines. In this way, the accuracy of wind power prediction can be developed further.

The wind farm is sometimes restricted to achieve full power rating due to turbine maintenance. When the corrective/preventive maintenance is implemented, the repair time might be extended when the wind speed is above a certain limit. The repair crew might be forbidden to climb the turbine tower due to weather issues (e.g. strong wind, icing problems). Hence, considering the influence of wind speed on turbine failure and repair, the wind speed is divided into three states.

- U_{L}: low wind speed, low failure rate, one crew is arranged to repair
- U_{M}: medium wind speed, failure rate increases, one crew is arranged to repair
- U_{H}: high wind speed, high failure rate, repair is not allowed

The failure and repair rate at different wind speed range is defined as:

- λ_{L}: failure rate at low wind speed
- λ_{M}: failure rate at medium wind speed
- λ_{H}: failure rate at high wind speed
- μ_{L}: repair rate at low wind speed
- μ_{M}: repair rate at medium wind speed
- μ_{H}: repair rate at high wind speed

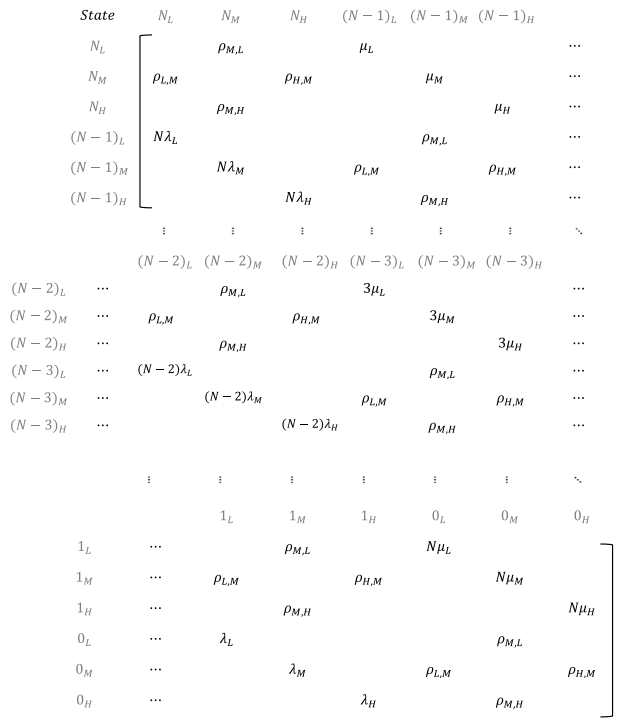

Fig. 3. State transition matrix for the Markov chain model.

The transition rates between different wind speed states can be defined as:

- $\rho_{\text{L,M}}$: transition rate from low to medium wind speed
- $\rho_{\text{M,L}}$: transition rate from medium to low wind speed
- $\rho_{\text{M,H}}$: transition rate from medium to high wind speed
- $\rho_{\text{H,M}}$: transition rate from high to medium wind speed

After classifying the data according to the wind speed range, the WT failure and repair rate under low, medium and high wind speed is calculated using Eqs. (12) and (13). The transition rate is calculated using Eq. (17),

$$\rho_{\text{i,j}} = \frac{N_{\text{i,j}}}{D_{\text{i}}} \tag{17}$$

where $N_{\text{i,j}}$ is the number of transitions from state i to state j and D_{i} is the duration of state i before switching to other states.

Using the parameters shown above, the state transition matrix for the Markov model is shown in Fig. 3. In the Markov model, $\lambda_{\text{L}} \neq \lambda_{\text{M}} \neq \lambda_{\text{H}}$ due to the variation of wind speed. The repair rate varies ($\mu_{\text{L}} \neq \mu_{\text{M}} \neq \mu_{\text{H}}$) since the turbine maintenance might be postponed due to the extreme weather conditions (e.g. fierce wind, icing).

The probability distribution $f(x)_{\text{L}}$, $f(x)_{\text{M}}$ and $f(x)_{\text{H}}$ that describes the number of operational turbines under low, medium and high wind speed is calculated based on the Markov model. The number of operational turbines is generated using the pseudo-random number generator according to $f(x)_{\text{L}}$, $f(x)_{\text{M}}$ and $f(x)_{\text{H}}$. In this way, the real-time number of operational turbines, N_{L}, N_{M} and N_{H} in time series under different wind states is simulated. The improved estimated wind power output $P_{(\text{wif})+\text{Markov}}$ from the wind farm, which considers the influence of turbine availability under different wind speed, can be calculated as:

$$P_{(\text{wif})+\text{Markov}} = P_{\text{L}} N_{\text{L}} + P_{\text{M}} N_{\text{M}} + P_{\text{H}} N_{\text{H}} \tag{18}$$

2.3. Transformer thermal model

The degradation rate of the transformers is determined by the operating temperature. Two corresponding variables, hot spot temperature

Table 1
Thermal characteristics.

For exponential equations in ONAF mode	Value
Exponential power of total losses versus top-oil (in tank) temperature rise (oil exponent)	$x = 0.8$
Exponential power of current versus winding temperature rise (winding exponent)	$y = 1.3$
For thermal upgraded paper in ONAF mode free from air at 1.5% moisture condition	**Value**
Pre-exponential factor	$A = 3.0 \times 10^4$ h^{-1}
Activation energy	$E_A = 86$ kJ/mol
Rated top oil temperature rise	$\Delta\theta_{o,r} = 52.8$ K
Rated winding gradient	$g_r = 12.8$ K
Rated hot spot factor	$H = 1.43$
Ratio of load loss over no-load loss	$R = 13.74$

(HST) and top oil temperature (TOT), reflect the heat dissipation from winding to oil and from oil tank to the surrounding air respectively due to the eddy loss (Kulkarni and Khaparde, 2017; Rommel et al., 2021). IEEE standard (Anon, 2012) indicates that transformers (with thermally upgraded insulation paper) operating the winding HST of 110 °C has a life expectancy of about 20 years. In this paper, simplified equivalent thermal circuits in the standard (Anon, 2018b) is used instead to estimate the HST and evaluate the aging rate of transformers.

According to Anon (2018b), the lifetime duration of WFET is determined by the insulation paper of the chosen transformer. The expected lifetime of the insulation paper mostly depends on the variation of ambient temperature and transformer load, i.e. the real-time generated power from the wind farm. Due to the failure and maintenance of WTs, even at high wind speed, the load of WFET cannot always reach the power rating of the connected wind farm. A thermal model is built to assess the impact of the variation of transformer load and ambient temperature on the transformer insulation.

A scenario is assumed to calculate the aging rate of the chosen WFET. In this case, a mineral-oil-filled transformer is assumed to operate in ONAF (Oil Natural Air Forced) mode and the thermal upgraded paper is chosen for transformer insulation. The thermal characteristics of the upgraded insulation paper (free from air at 1.5% moisture condition) are referred from Laneryd and Gustafsson (2020), in which a transformer is designed for wind power application and working in ONAF cooling mode. The thermal characteristics and the assigned values used in the equations are shown in Table 1.

Overloading a transformer accelerates the aging of transformer insulation paper. The risk of overloading is reflected by the HST of the transformer. To calculate the real-time HST, the load factor K in Eq. (6) is used as an input to reflect the variation of the generated power. To observe the variation of insulation paper lifetime with the change of installed capacity (i.e. adding turbines at the wind farm expansion stage), an expansion factor β is set to simulate the variation of the wind farm installed capacity in the expansion stage,

$$K_\beta = \beta K \tag{19}$$

where $\beta \in [1, 1.8]$ in this paper. According to IEC thermal model (Anon, 2018b), the real-time HST θ_h can be calculated as,

$$\theta_h = \theta_a + \Delta\theta_{o,r}\left(\frac{1 + {K_\beta}^2 R}{1 + R}\right)^x + H g_r {K_\beta}^y \tag{20}$$

where θ_a is the ambient temperature.

To estimate the expected lifetime of the insulation paper needs based on data over a certain period with variable ambient temperature, the weighted temperature equation (Martin et al., 2015) is used to derive the weighted hot spot temperature (HST, °C) over this period, as shown in Eq. (21),

$$\theta_{\mathrm{h_W}} = \frac{1}{\left[-\frac{R}{E_A}\ln\left(\frac{1}{T}\sum e^{\left(-\frac{E_A}{R(\theta_{h,i}+273)}\right)}\right)\right]} - 273 \tag{21}$$

where $\theta_{h,i}$ is the hot-spot temperature in the i_{th} 10-min interval. If the yearly profile of the transformer load is defined as a cycle and count the number of cycles throughout its lifetime, the life expectancy of the thermally upgraded paper t_{exp} (Anon, 2018b) based on the measured data in this period can be calculated as,

$$t_{\mathrm{exp}} = \frac{\frac{1}{DP_{\mathrm{end}}} - \frac{1}{DP_{\mathrm{start}}}}{A \cdot 24 \cdot 365} \cdot \exp\left[\frac{E_A}{R(\theta_{\mathrm{hW}} + 273)}\right] \tag{22}$$

where R is a gas constant equal to 8.314 J/(K mol); The insulation DP value at the end of life criterion or the moment of the sampling $DP_{\mathrm{end}} = 200$; The initial insulation DP value $DP_{\mathrm{start}} = 1000$.

Since the official regulation about service lifetime of transformers varies in each country, a relative aging rate is calculated instead to evaluate the transformer lifetime. According to IEC thermal model (Anon, 2018b), the aging rate of the paper insulation is given as follows:

$$k = A \cdot \exp\left[-\frac{E_A}{R(\theta_{\mathrm{h}} + 273)}\right] \tag{23}$$

A rated insulation condition "free from air and 0.5% moisture" is defined in the standard for thermally upgraded paper. The relative aging rate is defined to relate the aging rate at a certain insulation condition to the rated rate (Susa et al., 2011):

$$V = \frac{k}{k_r} = \frac{A}{A_r}\exp\left[\frac{1}{R}\cdot\left(\frac{E_{A_r}}{R(\theta_{\mathrm{h_r}} + 273)} - \frac{E_A}{R(\theta_{\mathrm{hW}} + 273)}\right)\right] \tag{24}$$

The value of V reflects the aging rate of the transformer. If $V = 1$, the transformer in the analyzed case has the same aging rate as in the rated condition. If $V > 1$, the transformer in the analyzed case is aging faster than in the rated condition, and vice versa.

3. Validation & discussion

3.1. Data analysis

In this section, the available data is classified according to the dominant factor influencing the load profile of WFETs at each moment. There are multiple factors influencing the power generation of a wind farm. Apart from the persistent wake effect, three other factors, in which each shows an evident impact on the load profile of WFETs, are discussed in this paper. The data is classified according to the dominant factor influencing the power generation at each unit time period.

- Type I — icing: turbine operation during winter is more likely to be influenced by icing.
- Type II — wind power curtailment: the power generation is operationally reduced below what the system is capable of producing (Qi et al., 2018).
- Type III — turbine availability: the output of turbine is zero or negative (due to the self-consumption of wind turbine) when the turbine is under failure or maintenance.
- Type IV — wake effect: all the turbines are in service and only influenced by the wake effect.

Next, using the algorithm shown in Fig. 4, the data can be classified according to the influence factors dominant at each moment. $U_{\mathrm{cut-in}}$ and $U_{\mathrm{cut-out}}$ indicate the cut-in and cut-out wind speed of the selected wind turbine. This classification assists in identifying the patterns and trends in the load profiles of WFETs by analyzing each type of data individually.

This paper focuses on analyzing the influence of type III+IV data on the load profile of WFETs. Type I and Type II data are noted, but not analyzed in depth since the impact of these two factors (icing and power curtailment) on transformer aging is limited. If a wind farm locates in a region when icing frequently occurs, the ambient

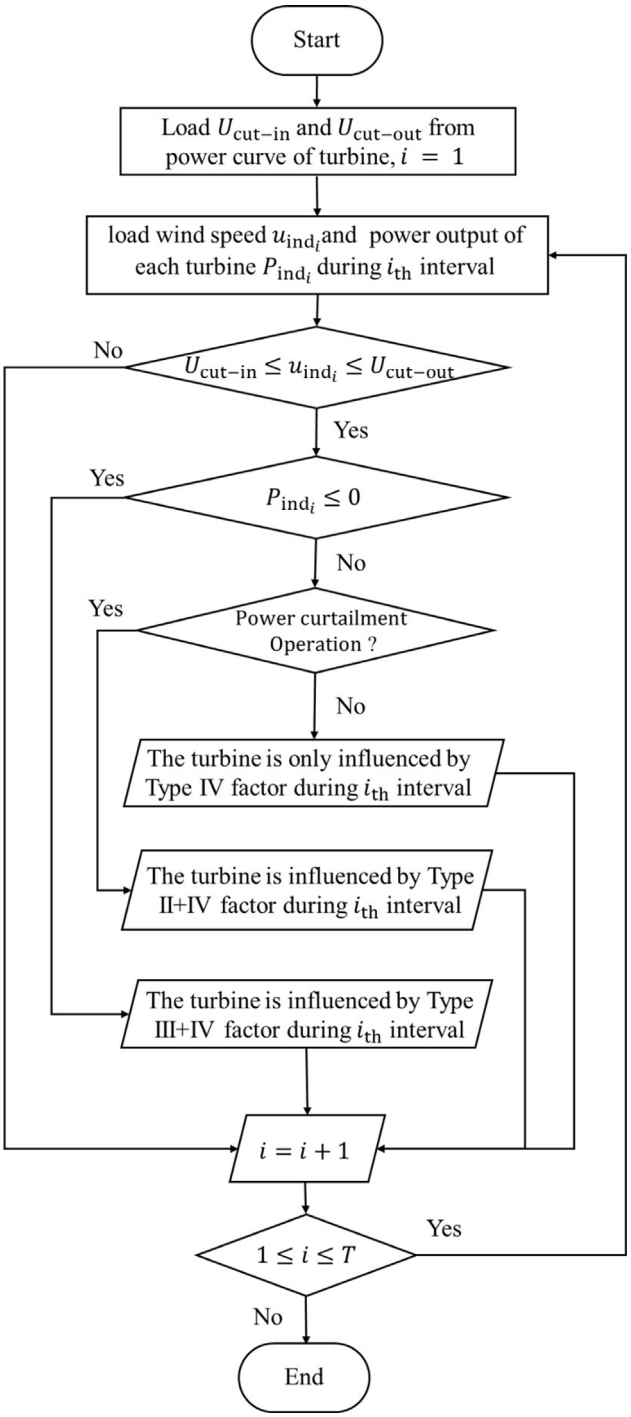

Fig. 4. Flow chart to label the data type (I:icing; II: power curtailment; III: turbine availability; IV: wake effect).

temperature and the icing accretion on the turbine blades restricts the raise of HST. For type II data, the analysis of power curtailment is outside the scope of this paper since it is more related to power system operation.

3.2. Case study

The proposed methodology is validated by comparing the simulation outcome with the measured data. The measurement record is from a wind farm called Stor-Rotliden (SRL). SRL is a 77.8 MW onshore wind farm with forest and semi-natural landscape, located in Vasterbotten, Sweden. The wind farm got commissioned in 2011, consisting of forty Vestas Wind Systems V90 turbines (eleven with rating of 1.8 MW and twenty-nine with rating of 2 MW).

Table 2
Data classification according to influencing factors.

factor / period	I	II	III	IV
2019/01/01-2019/12/31	32.88%	0.96%	25.78%	40.39%
2020/01/01-2020/12/31	32.88%	7.27%	15.29%	44.56%

The measurement record contains two year measured data from the wind farm based on a ten-minute interval (52560 measuring records in one year). The records include the following items.

- The measured wind speed from all turbines in the horizontal direction, U_{mea}, m/s
- The measured wind direction from all turbines in the horizontal direction, θ_{mea}, m/s
- Power curtailment setpoint at SRL in time sequence
- Ambient temperature of the turbine closest to the substation, θ_a, °C
- Active power output from SRL, P_{real}, MW

The curtailment setting record shows when the turbine rating is limited due to power curtailment operation. P_{real} is used to verify the accuracy of the model by comparing the simulation with the measured data. It is assumed that the turbine operation not in the period from 1st of March to 31st of October in each year is influenced by icing. Using the algorithm shown in Fig. 4, the data is classified according to the factors dominant at each measurement interval. The results are shown in Table 2.

The results in Table 2 show that for the SRL wind farm, the operation period influenced by the turbine availability is much longer compared to that influenced by the power curtailment. As stated in 3.1, Type I and Type II data is not included into analysis. Based on comparison with the 'filtered' measured data (Type III+IV), the influence of these factors on the load profile of transformers can be analyzed individually.

3.3. Validation of WIF method & wake model

Based on self-defined U_{nowake} (varying in $[5, 25]$, unit: m/s), wind direction θ_{nowake} (varying in $[0, 360]$, unit: degree) and the wind farm layout in Fig. 5, the wake impact factor (WIF) for SRL under different wind conditions is calculated using Eqs. (3) and (1). The WIF map at SRL is shown in Fig. 6. It is worth noting again that Fig. 6 reflects the reduction of the incoming wind speed under the assumption that the incoming wind direction θ_{nowake} is the same for each turbine.

Type IV data is used to check the accuracy of WIF and the Jensen wake model. Choosing the measured data from turbine B10 as an input $U_{mea_{B10}}$, the corrected incoming wind speed for the whole wind farm $U_{nowake(wif)}$ is calculated based on Eq. (4) and Fig. 6. Next, the Jensen model in Eq. (1) is used to calculate the reduced wind speed $U_{wake(wif)}$ of each turbine. The real-time power output of each turbine is derived by fitting the corresponding wind speed into the power curve of Vestas V90 in Fig. 8. As indicated in Section 2.3, the power output variables ($P_{nowake(wif)}$, $P_{wake(wif)}$, P_{real}) are converted into the corresponding load factors ($K_{nowake(wif)}$, $K_{wake(wif)}$, K_{real}) using Eq. (6). The simulation results and measured data are compared by the duration curve (load factor versus time), which is shown in Fig. 9(a) and Fig. 9(b). $K_{nowake(avg.)}$ in Figs. 9(a) and 9(b) indicate the calculated load factor assuming the wind speed of each turbine is the same as turbine B10 (the turbine chosen for WIF correction). MSE is calculated between

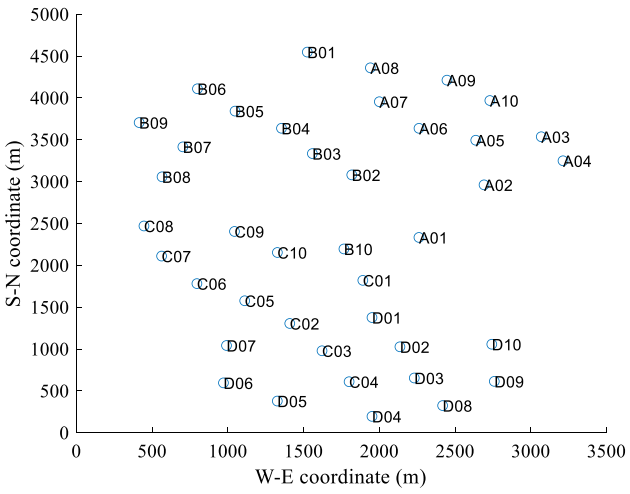

Fig. 5. Wind farm layout.

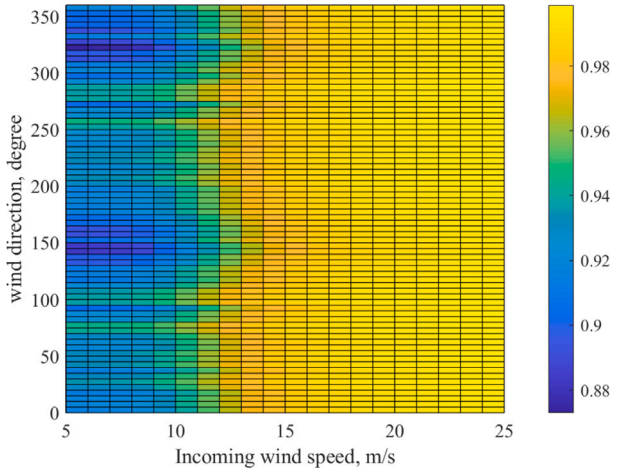

Fig. 6. Map of wake impact factor (WIF).

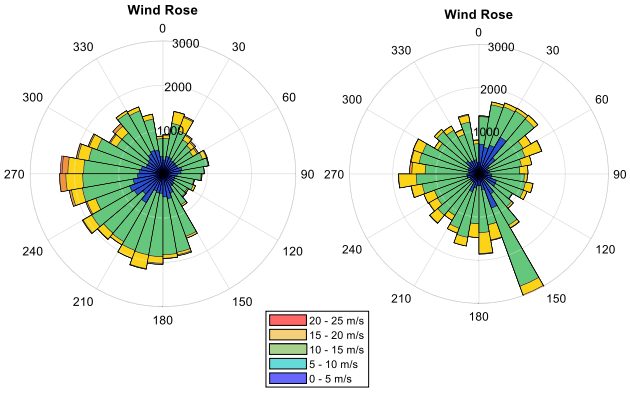

Fig. 7. Wind rose: (left) 2019; (right) 2020.

the simulation and measurement result and shown in Tables A.7 and A.8.

Besides, the effect of WIF and Jensen wake model correction can also be seen from the comparison of the annual energy production (AEP) of each turbine, which is shown in Figs. 10(a) and 10(b).

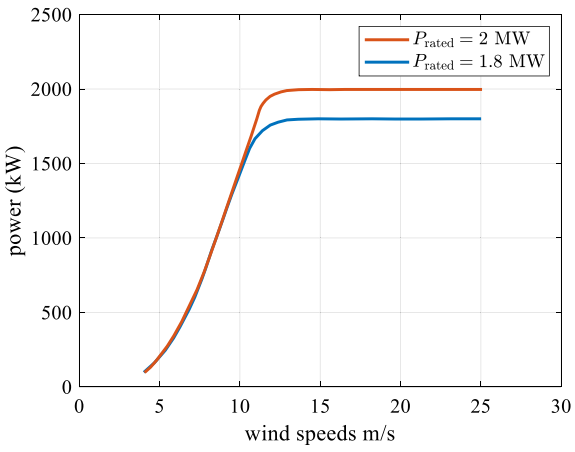

Fig. 8. Power curve of Vestas V90 (Anon, 2018c).

Table 3
WT failure & repair rate for BD model.

date / reliability	2019/03/01–2019/10/31	2020/03/01–2020/10/31
failure rate λ (occ./year)	22.56	15.38
repair rate μ (occ./year)	534.93	566.11
turbine availability q (%)	96.28%	97.28%

3.4. Validation of turbine availability model

After the verification of WIF and the Jensen wake model, the turbine availability is involved to see its influence on the load factor prediction. The data (type II+III+IV) is used in this case to guarantee the time continuity of data in the calculation of failure and repair date. Next, the data (type III+IV) are used to verify the accuracy of the proposed turbine availability model.

3.4.1. BD model

According to the output n and Z derived from the algorithm shown in Fig. 2, the failure and repair rates of turbines for the BD model in these two years are calculated using Eqs. (12)–(14) and the results are shown in Table 3.

Based on the binomial distribution curve generated by Eq. (15), random number is generated in time sequence according to the constant turbine availability q to simulate the variation of the operational turbines. The new duration curve considering the constant turbine availability is included in Figs. 11 and 12. Considering that this model is used to size the transformer, more attention should be paid to when the load factor is higher than 0.5. Hence, partial enlarged view is given to the time range of 0%–15%. The MSE between the simulation and the measurement is shown in Tables A.7 and A.8.

3.4.2. Markov model

To consider the variation of turbine availability under different wind conditions, the wind speed is divided into low, middle and high state. The range of low, middle and high wind speed defined in Arwade et al. (2011) is based on the average daily wind speed. In this paper, the three variables are defined according to U_{cut-in}, U_{rated} and $U_{cut-out}$ of the Vestas V90 power curve.

- U_L: Low wind speed (4.0–9.0 m/s)
- U_M: Medium wind speed (9.0–13.9 m/s)
- U_H: High wind speed (13.9–25.0 m/s)

After classifying the data according to the wind speed, n and Z under different wind speed state can be counted using the algorithm shown in Fig. 2. The failure and repair rate of the turbines under low,

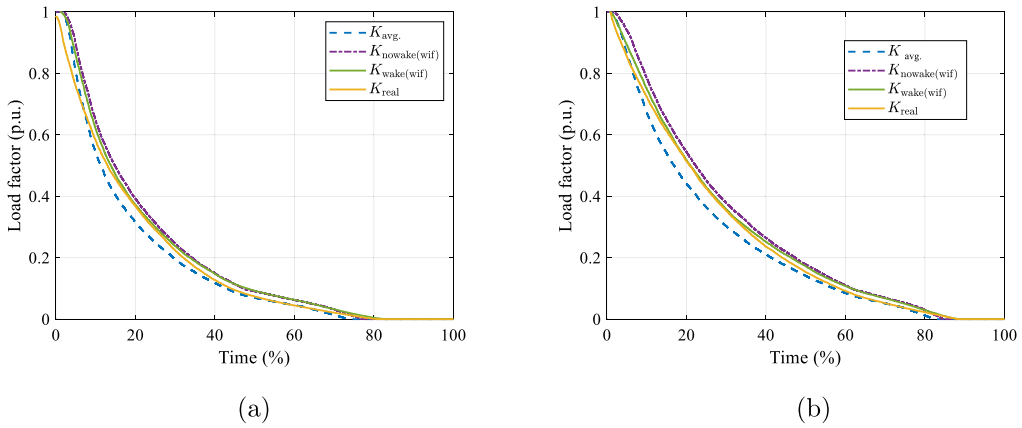

Fig. 9. Duration curve using WIF correction & Jensen model. in (a) 2019 (b) 2020.

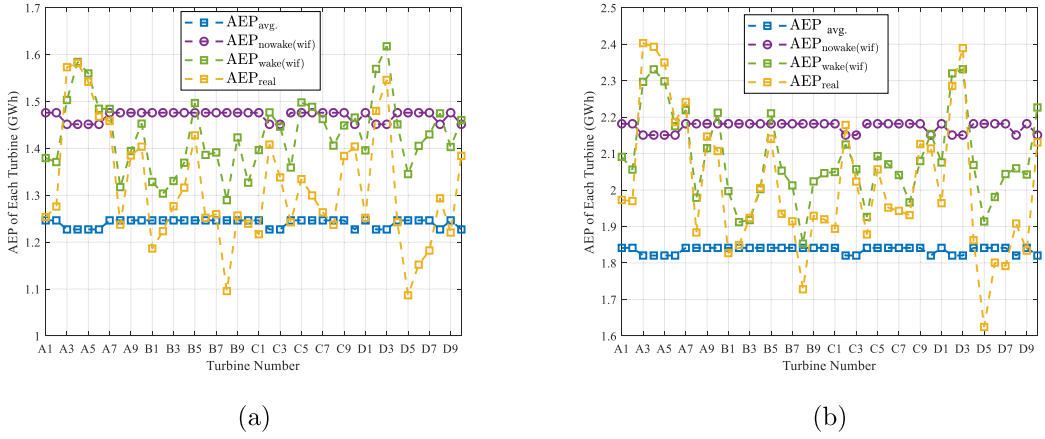

Fig. 10. Annual energy production of individual turbine in (a) 2019 (b) 2020.

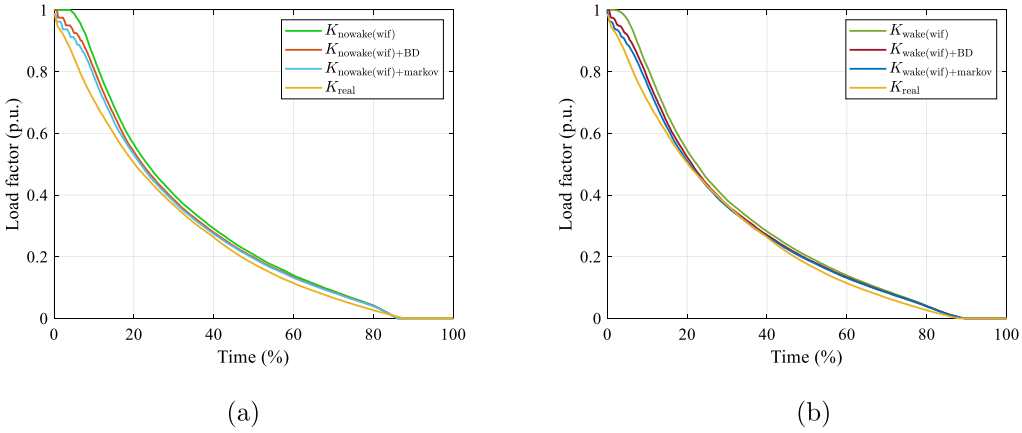

Fig. 11. Duration curve 2019 (a) nowake (b) wake.

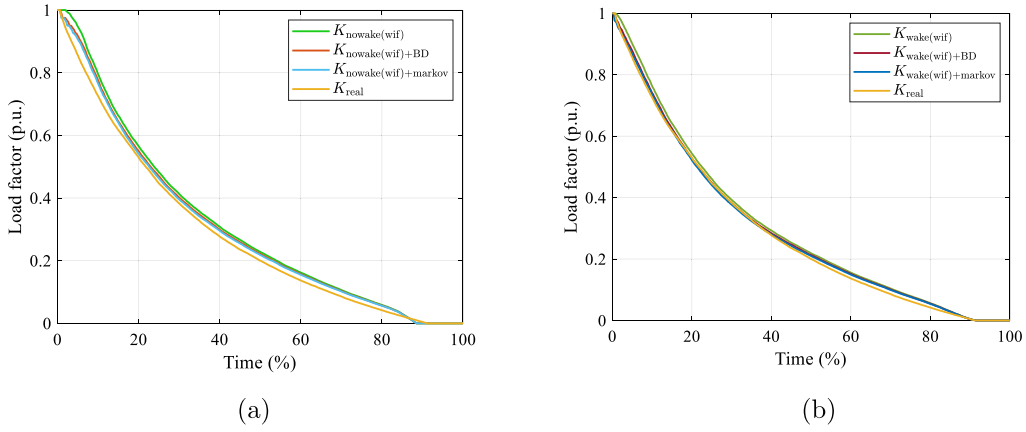

Fig. 12. Duration curve 2020 (a) nowake (b) wake.

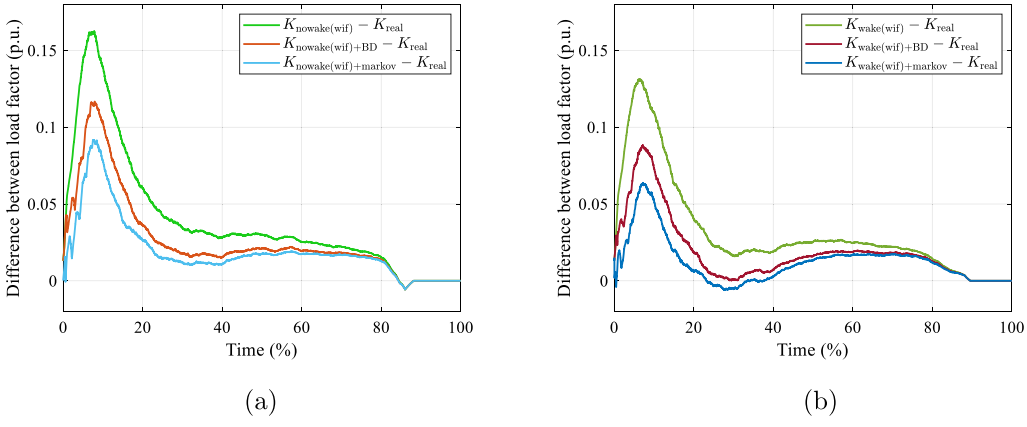

Fig. 13. Difference of duration curves between simulated cases and K_{real} in 2019 (a) nowake (b) wake.

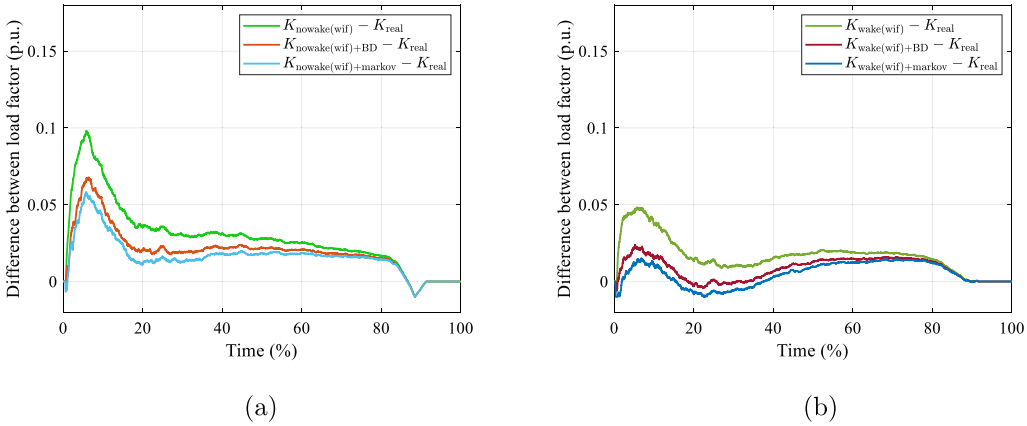

Fig. 14. Difference of duration curves between simulated cases and K_{real} in 2020 (a) nowake (b) wake.

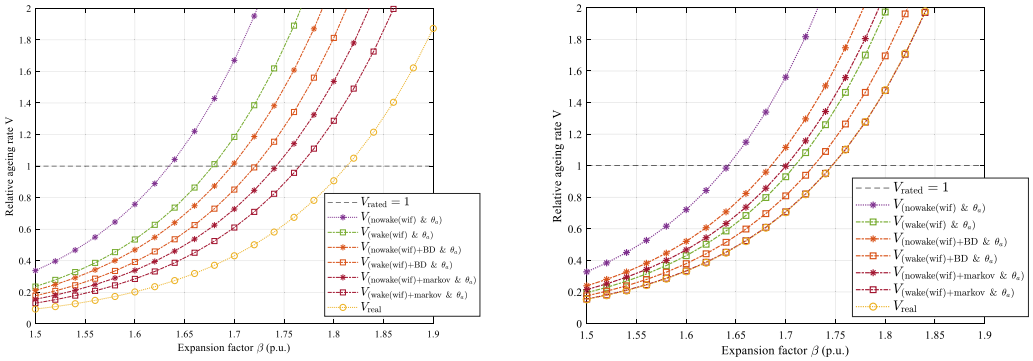

Fig. 15. Relative aging rate of transformer insulation lifetime versus expansion factor in (a) 2019 (b) 2020.

Table 4
WT failure & repair rate (2019) for Markov model.

Time	2019/03/01–2019/10/31		
wind state	U_L	U_M	U_H
failure rate λ (occ./year)	232.56	14.04	6.12
repair rate μ (occ./year)	6977.1	440.85	85.09
turbine availability q (%)	96.66	96.82	92.81

Table 5
WT failure & repair rate (2020) for Markov model.

Time	2020/03/01–2020/10/31		
wind state	U_L	U_M	U_H
failure rate λ (occ./year)	224.29	8.53	1.36
repair rate μ (occ./year)	7473.2	577.38	27.24
turbine availability q (%)	96.70	98.52	95.01

Table 6
Transition rates for Markov model.

Transition rates	$\rho_{L,M}$	$\rho_{M,L}$	$\rho_{M,H}$	$\rho_{H,M}$
2019/03/01–2019/12/31	769.64	3152.1	507.06	3400.2
2020/03/01–2020/12/31	809.82	2739.9	266.88	4134.7

middle and high wind speed are calculated using Eq. (12), Eq. (13) and Eq. (14) and the results are shown in Tables 4 and 5. Using Eq. (17), the transition rates between U_L, U_M and U_H are calculated and shown in Table 6. Random number is generated in time sequence according to the turbine availability q in each wind state to simulate the variation of the operational turbines. The new duration curve considering the changing turbine availability is included in Figs. 11 and 12. Since it is challenging to distinguish the curves due to the overlapping, the differences between $K_{\text{nowake(wif)}}$, $K_{\text{wake(wif)+BD}}$, $K_{\text{wake(wif)+markov}}$ and K_{real} are plotted in Figs. 13 and 14.

3.5. Transformer lifetime estimation

The data of the ambient temperature is selected from the database of SMHI, measured by a station at Fredrika, which is closest to Stor-Rotliden. Using Eqs. (20), (21) and (22), the relative aging rate of the transformer insulation is calculated and shown in Figs. 15(a) and 15(b).

3.6. Discussion

Combining the layout of wind farm (SRL) in Fig. 5 and the WIF map in Fig. 6, it can be seen that the wake effect influences the wind power generation especially when the wind speed is in 5–12 m/s and the wind direction is in [120, 180] and in [300, 340] degree. The wind farm suffers more wake loss in 2019 since Fig. 7 shows a more even distribution of the wind rose in 2020 than in 2019.

The WIF correction and the wake model improves the accuracy of wind power prediction. It can be seen in Figs. 9(a) and 9(b) that the simulated duration curves ($K_{\text{wake(wif)}}$ based on U_{wif}) fit the measured duration curve K_{real} better than the duration curve ($K_{\text{nowake(avg.)}}$ based on $U_{\text{avg.}}$). Tables A.7 and A.8 also show that the WMSE between K_{real} and $K_{\text{wake(wif)}}$ is the minimum. Besides, the simulated annual energy production (AEP) of each turbine fits better with the measured data in Figs. 10(a) and 10(b) after applying the WIF correction and the Jensen wake model.

It can be found in Figs. 9(a) and 9(b) that the wake effect reduces the load of WFETs and to some extent reduces the aging rate of WFETs according to Figs. 15(a) and 15(b). However, the influence of the wake effect is limited when the transformer is close to fully loaded. Hence, even the wake effect affects the aging rate, it is not the dominant factor influencing the HST of WFETs when the load is close to the installed capacity of the connected wind farms.

After considering the impact of the turbine availability using BD/Markov model, according to Figs. 13 and 14, the duration curve is corrected further. Combining with the MSE results shown in Tables A.9 and A.10, it shows that the simulation results using the Markov model fits the measured data better compared to the BD model since the BD model ignores the variation of turbine failure and repair rate. Tables 4 and 5 reflect that the correlation between the wind speed and the wind power generation is not strictly positive. High wind speed leads to a lower turbine availability compared to low or middle wind speed. The reduction of the operational turbines at high wind speed reduces the wind power generation and the load profile of the WFETs, especially when the wind speed satisfies the condition of generating power close to the installed capacity of the wind farm. This finding is beneficial for the DTR application since the hot spot temperature of transformer increases sharply when the WFET is fully loaded or overloaded. The decrease of turbine availability at high wind speed mitigates the risk of overloading transformers.

As can be seen from Figs. 15(a) and 15(b), the crosspoint between $V_{\text{nowake(wif)}}$ and V_{rated} indicates the transformer capacity would allow expansion of the wind farm by 63%. After considering the wake effect and turbine availability, the crosspoints between $V_{\text{wake(wif)+markov}}$ and V_{rated} indicate that the installed capacity of the wind farm could be increased by 74%–77% (11%–14% more than the $V_{\text{nowake(wif)}}$ case) in the expansion stage without causing the transformer aging rate higher than in the rated condition.

The inconsistency between K_{markov} and K_{real} can be due to the differences in operation and maintenance strategies between actual

implementation and the model's assumption (e.g. the defined range of low, middle and high wind speed, numbers of crews). The inconsistency may also arise due to the finite states included in the Markov model.

4. Conclusion

This paper proposes a new methodology to estimate the transformer load profile based on wind speed to improve the underutilization issue of the wind farm exported transformers (WFETs). The case study and discussion show that it is critical to incorporate turbine availability as well as wake effect analysis in order to get an accurate estimation of the load of transformers. The correction method (WIF) can pre-process limited wind data to eliminate the measurement error caused by the wake effect. The Markov model outperforms the BD model in predicting transformer loads by effectively incorporating the variable turbine availability. However, the BD model maintains its utility, offering a simpler evaluation of turbine availability's impact on load profiles due to its lower input requirements.

The results show that the changing turbine availability and the wake effect both reduce the aging rate of the WFETs, even the wake effect has limited influence when the transformer is close to fully loaded compared to the turbine availability. This methodology allows for a more accurate assessment of the aging rate of the existing transformers and the transformers in the planning stage. If components such as cables and breakers can be upgraded synchronously, it is possible to under-size the WFETs during the planning stage with the application of dynamic thermal rating. The WFETs can be better utilized based on a trade-off between economical cost and acceptable aging losses. After suitable parameter adjustments in the wake model, this methodology may also be applied to analyze the substation construction of offshore wind farms. As one of the heaviest components on offshore platforms, optimally rated export transformers help reduce construction costs and difficulty.

CRediT authorship contribution statement

Zhongtian Li: Conceptualization, Data curation, Formal analysis, Investigation, Methodology, Project administration, Resources, Software, Validation, Writing – original draft. **Patrik Hilber:** Project administration, Supervision, Visualization, Writing – review & editing. **Tor Laneryd:** Supervision, Writing – review & editing. **Gonzalo Pablo Navarro Diaz:** Resources, Writing – review & editing. **Stefan Ivanell:** Supervision, Writing – review & editing.

Declaration of competing interest

The authors declare that they have no known competing financial interests or personal relationships that could have appeared to influence the work reported in this paper.

Data availability

The authors do not have permission to share data.

Acknowledgments

Authors would like to thank François Besnard and Jan Henning Jürgensen from Vattenfall for providing data and technical support for this project.

Appendix. MSE comparison

See Tables A.7–A.9.

Table A.7
MSE between measurement and simulation (2019).

K_{real} \ K_{SIM}	$K_{avg.}$	$K_{nowake(wif)}$	$K_{wake(wif)}$
MSE with K_{real}	8.0228e−4	1.4704e−3	8.3118e−4

Table A.8
MSE between the measurements and simulations (2020).

K_{real} \ K_{SIM}	$K_{avg.}$	$K_{nowake(wif)}$	$K_{wake(wif)}$
MSE with K_{real}	1.1471e−3	9.5766e−4	2.3182e−4

Table A.9
WMSE between measurement and simulation (2019).

K_{real} \ K_{SIM}	$K_{nowake(wif)}$	$K_{wake(wif)}$
WMSE	2.0282e−3	1.3213e−3
K_{real} \ K_{SIM}	$K_{nowake(wif)+BD}$	$K_{wake(wif)+BD}$
WMSE	9.1862e−4	4.9855e−4
K_{real} \ K_{SIM}	$K_{nowake(wif)+Markov}$	$K_{wake(wif)+Markov}$
WMSE	4.8001e−4	2.0613e−4

Table A.10
WMSE between measurement and simulation (2020).

K_{real} \ K_{SIM}	$K_{nowake(wif)}$	$K_{wake(wif)}$
WMSE	7.5507e−4	2.1422e−4
K_{real} \ K_{SIM}	$K_{nowake(wif)+BD}$	$K_{wake(wif)+BD}$
WMSE	3.3077e−4	3.9764e−5
K_{real} \ K_{SIM}	$K_{nowake(wif)+Markov}$	$K_{wake(wif)+Markov}$
WMSE	2.2139e−4	2.3049e−5

References

Akhlaghi, M., Moravej, Z., Bagheri, A., 2022. Maximizing wind energy utilization in smart power systems using a flexible network-constrained unit commitment through dynamic lines and transformers rating. Energy 261, 124918.

Anon, 2012. IEEE guide for loading mineral-oil-immersed transformers and step-voltage regulators. IEEE Std C57.91-2011 (Revision of IEEE Std C57.91-1995), pp. 1–123. http://dx.doi.org/10.1109/IEEESTD.2012.6166928.

Anon, 2016. Reuse and recycling of wind turbines. Standard, swedish energy agency, URL: https://www.energimyndigheten.se/globalassets/fornybart/framjande-av-vindkraft/aterbruk-och-atervinning-av-vindkraftverk_webb-final.pdf.

Anon, 2018a. Ordinance on revenue framework for electricity network operations. Standard, Svensk författningssamling, URL: https://svenskforfattningssamling.se/sites/default/files/sfs/2018-08/SFS2018-1520.pdf.

Anon, 2018b. Power transformers - part 7: Loading guide for mineral-oil-immersed power transformers. Standard IEC 60076-7, International Electrotechnical Commission, URL: https://webstore.iec.ch/publication/34351.

Anon, 2018c. Vestas V90 gridstreamer. Standard, wind-turbine-models.com, URL: https://en.wind-turbine-models.com/turbines/248-vestas-[V90]-gridstreamer.

Anon, 2019. Wind energy generation systems - part 26-1: Availability for wind energy generation systems. Standard IEC 61400-26-1, International Electrotechnical Commission, URL: https://webstore.iec.ch/publication/62548.

Anon, 2022a. The declaration of energy ministers on the North Sea as a green power plant of Europe.

Anon, 2022b. The Marienborg declaration. In: The Baltic Sea Energy Security Summit.

Arguence, O., Cadoux, F., 2020. Sizing power transformers in power systems planning using thermal rating. Int. J. Electr. Power Energy Syst. 118, 105781.

Arwade, S.R., Lackner, M.A., Grigoriu, M.D., 2011. Probabilistic models for wind turbine and wind farm performance. J. Solar Energy Eng. 133 (4).

Bhaumik, D., Crommelin, D., Kapodistria, S., Zwart, B., 2018. Hidden Markov models for wind farm power output. IEEE Trans. Sustain. Energy 10 (2), 533–539.

Carroll, J., McDonald, A., McMillan, D., 2014. Reliability comparison of wind turbines with DFIG and PMG drive trains. IEEE Trans. Energy Convers. 30 (2), 663–670. http://dx.doi.org/10.1109/TEC.2014.2367243.

Daminov, I., Prokhorov, A., Caire, R., Alvarez-Herault, M.-C., 2021. Energy limit of oil-immersed transformers: A concept and its application in different climate conditions. IET Gener., Transm. Distribution 15 (3), 495–507.

de Sá Sarmiento, F.I.P., Oliveira, J.L.G., Passos, J.C., 2022. Impact of atmospheric stability, wake effect and topography on power production at complex-terrain wind farm. Energy 239, 122211.

Frandsen, S., Barthelmie, R., Pryor, S., Rathmann, O., Larsen, S., Højstrup, J., Thøersen, M., 2006. Analytical modelling of wind speed deficit in large offshore wind farms. Wind Energy: Int. J. Progress Appl. Wind Power Convers. Technol. 9 (1–2), 39–53.

Guo, N., Zhang, M., Li, B., Cheng, Y., 2021. Influence of atmospheric stability on wind farm layout optimization based on an improved Gaussian wake model. J. Wind Eng. Ind. Aerodyn. 211, 104548.

Hillary, W., Jayarathna, K., Ranasinghe, L., Samarakoon, S., Rathnayake, N., Lucas, J.R., Samarasinghe, R., 2017. A tool for estimating remaining life time of a power transformer. In: 2017 Moratuwa Engineering Research Conference (MERCon). pp. 373–378. http://dx.doi.org/10.1109/MERCon.2017.7980513.

Hou, P., Hu, W., Soltani, M., Chen, Z., 2015. Optimized placement of wind turbines in large-scale offshore wind farm using particle swarm optimization algorithm. IEEE Trans. Sustain. Energy 6 (4), 1272–1282.

Hou, P., Hu, W., Soltani, M., Chen, C., Zhang, B., Chen, Z., 2016. Offshore wind farm layout design considering optimized power dispatch strategy. IEEE Trans. Sustain. Energy 8 (2), 638–647.

Humayun, M., Safdarian, A., Degefa, M.Z., Lehtonen, M., 2015. Demand response for operational life extension and efficient capacity utilization of power transformers during contingencies. IEEE Trans. Power Syst. 30 (4), 2160–2169. http://dx.doi.org/10.1109/TPWRS.2014.2358687.

Ishihara, T., Yamaguchi, A., Fujino, Y., 2004. Development of a new wake model based on a wind tunnel experiment. Global Wind Power 105 (1), 33–45.

Iskender, I., Mamizadeh, A., 2011. An improved nonlinear thermal model for MV/LV prefabricated oil-immersed power transformer substations. Electr. Eng. 93 (1), 9–22.

Jensen, N.O., 1983. A Note on Wind Generator Interaction. vol. 2411, Citeseer.

Karki, R., Hu, P., Billinton, R., 2006. A simplified wind power generation model for reliability evaluation. IEEE Trans. Energy Convers. 21 (2), 533–540.

Katic, I., Højstrup, J., Jensen, N.O., 1986. A simple model for cluster efficiency. In: European Wind Energy Association Conference and Exhibition. Vol. 1, A. Raguzzi Rome, Italy, pp. 407–410.

Kazmi, S.H.H., Laneryd, T., Giannikas, K., Ahrenfeldt, S.F., Sørensen, T.S., Olesen, T.H., Holbøll, J., 2021. Cost optimized dynamic design of offshore windfarm transformers with reliability and contingency considerations. Int. J. Electr. Power Energy Syst. 128, 106684.

Kim, H., Singh, C., Sprintson, A., 2012. Simulation and estimation of reliability in a wind farm considering the wake effect. IEEE Trans. Sustain. Energy 3 (2), 274–282.

Kulkarni, S.V., Khaparde, S.A., 2017. Transformer Engineering: Design, Technology, and Diagnostics. CRC Press.

Lachman, M.F., Griffin, P.J., Walter, W., Wilson, A., 2003. Real-time dynamic loading and thermal diagnostic of power transformers. IEEE Trans. Power Deliv. 18 (1), 142–148.

Lai, C.-M., Teh, J., 2022. Comprehensive review of the dynamic thermal rating system for sustainable electrical power systems. Energy Rep. 8, 3263–3288.

Laneryd, T., Gustafsson, A., 2020. Dynamic thermal behaviour of wind power transformers. In: CIGRE Session-48, Paris 2020. (A2-103).

Larsen, G.C., 1988. A Simple Wake Calculation Procedure. Risø National Laboratory.

Leite, A.P., Borges, C.L., Falcao, D.M., 2006. Probabilistic wind farms generation model for reliability studies applied to Brazilian sites. IEEE Trans. Power Syst. 21 (4), 1493–1501.

Li, Y., Chen, Q., Strbac, G., Hur, K., Kang, C., 2023. Active distribution network expansion planning with dynamic thermal rating of underground cables and transformers. IEEE Trans. Smart Grid 1. http://dx.doi.org/10.1109/TSG.2023.3266782.

Li, Z., Morozovska, K., Hilber, P., Laneryd, T., Ivanell, S., 2021a. Sizing transformer considering transformer thermal limits and wind farm wake effect. In: 2021 IEEE PES Innovative Smart Grid Technologies - Asia (ISGT Asia). pp. 1–5. http://dx.doi.org/10.1109/ISGTAsia49270.2021.9715702.

Li, Y., Wang, Y., Chen, Q., 2021b. Optimal dispatch with transformer dynamic thermal rating in ADNs incorporating high PV penetration. IEEE Trans. Smart Grid 12 (3), 1989–1999. http://dx.doi.org/10.1109/TSG.2020.3037874.

Long, H., Zhang, Z., 2015. A two-echelon wind farm layout planning model. IEEE Trans. Sustain. Energy 6 (3), 863–871.

Manco, T., Testa, A., 2007. A Markovian approach to model power availability of a wind turbine. In: 2007 IEEE Lausanne Power Tech. IEEE, pp. 1256–1261.

Manwell, J.F., McGowan, J.G., Rogers, A.L., 2010. Wind Energy Explained: Theory, Design and Application. John Wiley & Sons.

Martin, D., Cui, Y., Ekanayake, C., Ma, H., Saha, T., 2015. An updated model to determine the life remaining of transformer insulation. IEEE Trans. Power Deliv. 30 (1), 395–402. http://dx.doi.org/10.1109/tpwrd.2014.2345775.

Nguyen, N., Almasabi, S., Mitra, J., 2019. Impact of correlation between wind speed and turbine availability on wind farm reliability. IEEE Trans. Ind. Appl. 55 (3), 2392–2400.

Nguyen, N., Mitra, J., 2017. Reliability of power system with high wind penetration under frequency stability constraint. IEEE Trans. Power Syst. 33 (1), 985–994.

Pakenham, B., Ermakova, A., Mehmanparast, A., 2021. A review of life extension strategies for offshore wind farms using techno-economic assessments. Energies 14 (7), 1936.

Porté-Agel, F., Bastankhah, M., Shamsoddin, S., 2020. Wind-turbine and wind-farm flows: A review. Boundary-layer Meteorol. 174 (1), 1–59.

Qi, Y., Dong, W., Dong, C., Huang, C., 2018. Fixing wind curtailment with electric power system reform in China. In: China's Energy in Transition Series. Brooking-Tsinghua Center for Public Policy, Beijing.

Radünz, W.C., Sakagami, Y., Haas, R., Petry, A.P., Passos, J.C., Miqueletti, M., Dias, E., 2021. Influence of atmospheric stability on wind farm performance in complex terrain. Appl. Energy 282, 116149.

Rommel, D., Di Maio, D., Tinga, T., 2021. Transformer hot spot temperature prediction based on basic operator information. Int. J. Electr. Power Energy Syst. 124, 106340.

Sayas, F.C., Allan, R., 1996. Generation availability assessment of wind farms. IEE Proc., Gener. Transm. Distrib. 143 (5), 507–518.

Simonson, E., Lapworth, J., 1995. Thermal capability assessment for transformers. In: Second International Conference on the Reliability of Transmission and Distribution Equipment, 1995. IET, pp. 103–108.

Song, Z., Zhang, Z., Chen, X., 2016. The decision model of 3-dimensional wind farm layout design. Renew. Energy 85, 248–258.

Spinato, F., Tavner, P.J., Van Bussel, G.J., Koutoulakos, E., 2009. Reliability of wind turbine subassemblies. IET Renew. Power Gener. 3 (4), 387–401.

Sulaeman, S., Benidris, M., Mitra, J., Singh, C., 2017. A wind farm reliability model considering both wind variability and turbine forced outages. IEEE Trans. Sustain. Energy 8 (2), 629–637. http://dx.doi.org/10.1109/TSTE.2016.2614245.

Susa, D., Lehtonen, M., Nordman, H., 2005. Dynamic thermal modelling of power transformers. IEEE Trans. Power Deliv. 20 (1), 197–204.

Susa, D., Liland, K., Lundgaard, L., Vårdal, G., 2011. Generator step-up transformer post mortem assessment. Eur. Trans. Electr. Power 21 (5), 1802–1822.

Tao, S., Xu, Q., Feijóo, A., Zheng, G., 2020. Joint optimization of wind turbine micrositing and cabling in an offshore wind farm. IEEE Trans. Smart Grid 12 (1), 834–844.

Tavner, P., Edwards, C., Brinkman, A., Spinato, F., 2006. Influence of wind speed on wind turbine reliability. Wind Eng. 30 (1), 55–72.

Tavner, P., Greenwood, D., Whittle, M., Gindele, R., Faulstich, S., Hahn, B., 2013. Study of weather and location effects on wind turbine failure rates. Wind Energy 16 (2), 175–187.

Tavner, P., Xiang, J., Spinato, F., 2007. Reliability analysis for wind turbines. Wind Energy: Int. J. Progr. Appl. Wind Power Convers. Technol. 10 (1), 1–18.

Teh, J., Lai, C.-M., Muhamad, N.A., Ooi, C.A., Cheng, Y.-H., Zainuri, M.A.A.M., Ishak, M.K., 2018. Prospects of using the dynamic thermal rating system for reliable electrical networks: A review. IEEE Access 6, 26765–26778.

Tripathy, S.C., Lakervi, E., 2005. Evaluation of transformer overloading capability. Eur. Trans. Electr. Power 15 (5), 455–464.

Turnell, A.V., Linnet, A., Tamadon, N., Morozovska, K., Hilber, P., Laneryd, T., Wihlen, M., 2018. Risk and economic analysis of utilizing dynamic thermal rated transformer for wind farm connection. In: 2018 IEEE International Conference on Probabilistic Methods Applied To Power Systems (PMAPS). IEEE, pp. 1–6.

Viafora, N., Morozovska, K., Kazmi, S.H.H., Laneryd, T., Hilber, P., Holbøll, J., 2019. Day-ahead dispatch optimization with dynamic thermal rating of transformers and overhead lines. Electr. Power Syst. Res. 171, 194–208.

Wallnerström, C.J., Hilber, P., 2014. Reliability analysis and asset management applied to power distribution.

Wang, Q., Luo, K., Wu, C., Zhu, Z., Fan, J., 2022. Mesoscale simulations of a real onshore wind power base in complex terrain: Wind farm wake behavior and power production. Energy 241, 122873.

Wu, Y.-K., Lee, C.-Y., Chen, C.-R., Hsu, K.-W., Tseng, H.-T., 2013. Optimization of the wind turbine layout and transmission system planning for a large-scale offshore windfarm by AI technology. IEEE Trans. Ind. Appl. 50 (3), 2071–2080.

Yang, K., Kwak, G., Cho, K., Huh, J., 2019. Wind farm layout optimization for wake effect uniformity. Energy 183, 983–995.

Yang, X., Sotiropoulos, F., 2016. Analytical model for predicting the performance of arbitrary size and layout wind farms. Wind Energy 19 (7), 1239–1248.

Yang, H., Xie, K., Tai, H.-M., Chai, Y., 2015. Wind farm layout optimization and its application to power system reliability analysis. IEEE Trans. Power Syst. 31 (3), 2135–2143.

Zarei, T., Morozovska, K., Laneryd, T., Hilber, P., Wihlen, M., Hansson, O., 2019. Reliability considerations and economic benefits of dynamic transformer rating for wind energy integration. Int. J. Electr. Power Energy Syst. 106, 598–606.

Zhan, L., Letizia, S., Valerio Iungo, G., 2020. Lidar measurements for an onshore wind farm: Wake variability for different incoming wind speeds and atmospheric stability regimes. Wind Energy 23 (3), 501–527.

Zigras, D., Moennich, K., 2006. Farm efficiencies in large wind farms. Deutsches Windenergie-Institut (DEWI).